A Reaction-Transport-Mechanical Approach to Modeling the Interrelationships Among Gas Generation, Overpressuring, and Fracturing: Implications for the Upper Cretaceous Natural Gas Reservoirs of the Piceance Basin, Colorado[1]

Dorothy F. Payne,[2] Kagan Tuncay,[3] Anthony Park,[3] John B. Comer,[4] and Peter Ortoleva[3]

ABSTRACT

Predicting reservoir characteristics in tight-gas sandstone reservoirs, such as those of the Upper Cretaceous units of the Piceance basin, is difficult due to the interactions of multiple processes acting on sediments during basin development. To better understand the dynamics of these systems, a forward numerical model, which accounts for compaction, fracturing, hydrocarbon generation, and multiphase flow (BasinRTM) is used in a one-dimensional simulation of the U.S. Department of Energy's Multiwell Experiment (MWX) site in the Piceance basin. Of particular interest is the effect of gas generation on the dynamics of the system.

Comparisons of predicted present-day and observed reservoir characteristics show that the simulation generally captures the observed patterns. Analysis of the simulated history of the MWX site shows that rheologic properties constrain the distribution of fractures, whereas the fracture dynamics are controlled by the dynamics of the stress and fluid pressure histories. Results suggest that gas generation is not necessary to induce fracturing; however, by contributing to overpressure it has two important implications: (1) during maximum burial, gas saturation in one unit affects fracturing in other units, thereby contributing to the creation of flow conduits through which gas may migrate and (2) gas saturation helps sustain overpressure during uplift and erosion, allowing fractures to remain open.

INTRODUCTION

The purpose of this study is to examine the interactions among gas generation, overpressuring, and fracturing during the development of tight-gas sandstone reservoirs. This is accomplished using a forward numerical reaction-transport-mechanical (RTM) simulator for sedimentary basins, called BasinRTM. The study case is a one-dimensional simulation of the U.S. Department of Energy's Multiwell Experiment (MWX) site in the Piceance basin of western Colorado.

Due to their unconventional nature, exploration for and exploitation of producible reservoirs in fractured, low-matrix permeability rocks, such as those found in the Upper Cretaceous units of the Piceance basin, are difficult and production problems are common. Two specific difficulties are (1) predicting the location and extent of fracture networks or compartments and (2) predicting the timing and geometry of generation and migration of natural gas with respect to the development of fractures. Most approaches to these problems consider present-day characteristics to determine the likely areas of fracturing (major structural features) and gas generation (high maturity and abundance of source rock). For the Piceance basin, several studies have integrated present-day basin properties to predict the locations of fracture networks and gas-bearing reservoirs in

the Piceance basin. Lorenz et al. (1993) used an analysis of in situ stresses and known fracture distribution to develop a basin stress history, which is then used to predict likely zones of fracturing. This information presumably then may be combined with information on the geometry of likely source rocks and the timing of gas generation to create an overlay that will suggest likely areas for producible reservoirs. Hoak and Klawitter (1997) assumed that central Piceance basin Mesaverde strata are gas saturated, and used a variety of geologic maps, seismic data, well data, and remote data to identify the location of major basement faults and subsurface structures, which they suggested to be directly related to fracturing and the development of fracture zones. Tyler et al. (1996) integrated hydrodynamic studies with extensive data on source rock geometry, abundance, and thermal maturity to establish critical controls on productive reservoirs. These studies all used present-day basin properties and the intersection of important criteria to predict likely producible reservoirs.

This kind of approach, however, is limited because there are productive areas that are not spatially associated with major structures or high maturity or abundance of source rocks, and there are unproductive areas that are spatially associated with these indicators. To improve predictability, one would want to better understand the complex interaction of processes that lead to the development of such reservoirs. For example, the generation of gas and its transport may be integral to the development of reservoirs in the Piceance basin and similar basins. Lorenz and Finley (1991) noted that elevated pore fluid pressures may be a necessary component in the development of fractures in the Piceance basin, and this relationship has been suggested elsewhere (Hunt, 1990; Cartwright, 1994; Maubege and Lerche, 1994; Pitman and Sprunt, 1986; Roberts and Nunn, 1995; Wang and Xie, 1998). The generation of hydrocarbons is suggested to contribute to the creation of overpressure in sedimentary basins (Hedberg, 1974; Luo and Vasseur, 1996). Specifically in the Piceance basin, as well as other uplifted Rocky Mountain basins, Spencer (1987) suggested that the most likely explanation for present-day elevated pore fluid pressures is the generation of natural gas. This implies that, in the case of fractured natural gas reservoirs such as those that exist in the Piceance basin, the generation of natural gas may contribute to the creation of the reservoirs in which it is contained. This notion is explored in this paper as it has implications for the location and extent of producible reservoirs in these types of settings.

Clearly, the multitude of processes and their interactions complicate matters. Gas generation may be one of many factors that contribute to overpressure, including fluid thermal expansion, compaction, permeability, and relative permeabilities under multiphase flow conditions. These factors are influenced by the burial, thermal, and tectonic histories. Likewise, overpressure may be one of several factors important in fracturing. Rheologic properties and imposed vertical and lateral stresses are also important. In addition, many of the processes occurring during basin development are strongly coupled. For example, gas generation may contribute to overpressure, which may contribute to fracturing. Fracturing, in turn, increases permeability, facilitating the escape of the gas and resulting in reduced fluid pressure. This will ultimately inhibit the development of, or even seal, fractures. Many such coupling relationships exist, and they diminish the utility of using simple correlations to locate productive areas.

One approach to better understand the occurrence of such reservoirs is forward modeling of the processes that contribute to their development over the history of a sedimentary basin. The objective here is to use this approach to simulate the development of a sedimentary basin using the BasinRTM simulator, which accounts for the multitude of basin processes and their interactions through time. Mathematical equations conserving mass, energy, and momentum describe each of the processes and their interdependencies, whereas thermal and burial/uplift histories are imposed to control the conditions at the boundaries of the basin. The processes simulated in this modeling study include burial and sedimentation, uplift and erosion, compaction, organic diagenesis and gas generation, fracturing, and multiphase flow. The rock properties and their distributions that are computed by the simulator include temperature, fluid pressure, fluid composition, fracture locations and characteristics, porosity and permeability (fracture and matrix components of each), and stresses.

The modeling approach implemented in BasinRTM is based on two important principles: using fundamental laws of chemistry and physics, in favor of empirical relationships, to describe more complex geological processes; and full coupling of the processes to capture important feedback relationships. Empirical relationships are problematic because they are usually locally specific, they represent a composite of fundamental processes, and they may describe a relationship between processes that are only indirectly physically related; hence, they have limited applicability to the wide range of geologic settings. As an example, porosity is often assumed to be a function of depth, and a well-studied, locally specific porosity/depth relation is often used to predict porosity in a different location. Realistically, porosity is more accurately a function of compaction and cementation, which is affected by lithologic characteristics, and which is a function

of the detailed history of the rates of burial and uplift, fluid flow, mineral-pore fluid reactions, such as dissolution and precipitation, and other processes. Thus an empirical porosity/depth correlation from one location may incorrectly describe that of another location. By considering the physical and chemical laws that determine the porosity and other characteristics, a model can be appropriately tailored for a specific basin.

Basin deformation analysis requires an accounting of the coupling of the many operating, interacting RTM processes. For example, pore fluid pressure affects stresses, changes in stresses can lead to fracturing, and fracturing, in turn, affects pore fluid pressure. Additionally, rocks fracture due to the difference between the fluid pressure and the least compressive stress; however, as fractures open, the overall rock volume increases and fluid pressure in the fractures compresses the rock, increasing the compressive stress normal to the fracture plane and reducing the rate of fracture growth. Thus fracturing is a self-limiting process. These effects can only be studied by solving the stress, deformation, fracturing, and fluid flow simultaneously.

In this study, we simulate the history of the MWX site in the Rulison field of the south-central Piceance basin from the Cretaceous to the present (Figure 1). The MWX site lends itself well to this study because there is abundant data to use as input and with which to compare simulation results. The MWX site was designed by the U.S. Department of Energy in the 1970s to characterize these types of unconventional reservoirs and to study technologies to better exploit them. This paper is part of ongoing research to develop a forward-modeling approach to optimize exploration and production strategies for tight-gas sandstone reservoirs. The results presented here are not intended to be used to precisely predict productive zones, rather they are to be used to illustrate the complex nature of the processes that combine to create these types of reservoirs and to consider the relative impacts of individual processes, in particular gas generation.

THE BASINRTM SIMULATOR

The model is based on the finite element solution of equations of rock deformation, fracture network statistical dynamics, rock failure, multiphase flow, organic diagenesis, mechanical compaction, and heat transfer. The RTM equations are solved consistently with the influences at the boundary of the basin (sedimentation/erosion, basement heat flux, climate, sea level, and extension/compression or uplift/subsidence history). External influences (transient boundary conditions) are allowed to influence the progress of internal RTM processes.

Within the basin, these RTM processes modify the sediment chemically and mechanically to arrive at the internal distribution of physical and chemical characteristics. BasinRTM makes its predictions in a completely self-consistent way through a set of multiphase, organic and inorganic, reaction-transport modules. The scope of this paper precludes a detailed treatment of the simulator, but qualitative descriptions of the calculations of relevant phenomena and processes follow.

Gas Generation

To account for the generation of natural gas, a new chemical kinetic approach is used to model the thermal maturation of gas-prone kerogen (Payne, 1998). In this model, natural gas speciation is based on observed structural transformations of proto-kerogen molecules in naturally matured samples. In this approach compositionally specific reactants evolve to specific intermediate and mobile products through balanced nth order processes by way of a network of sequential and parallel reactions. This model predicts natural gas speciation and relative reaction rates, which have important implications for natural gas resource assessment. The kinetics of the reactions in the reaction network are calibrated on the geochemistry and thermal indicators of Mesaverde Group coals from the MWX site, under the assumption that these coals are derived primarily from lignin. The reaction network comprises 26 species and 22 reactions. Each species has a unique chemical formula and a unique set of reactions for which it is a product and for which it is a reactant. Most of these species are immobile intermediate species, defunctionalized or fragmented parts of the lignin structure; the mobile species include H_2O, CO_2, CH_4, and H_2. The set of unique parameters for each reaction includes stoichiometric coefficients and an activation energy. The network of reactions is tabulated then used to construct a matrix of reactions used in the speciation computations. The reactions are thermally dependent. This model has been applied to the MWX site independently of the RTM model, and results show that for the thermal history of the MWX site natural gas is generated until about 25 Ma, and then the combination of cooling temperatures associated with uplift and the exhaustion of the generation potential of the source rocks caused gas generation to cease at this location in these strata (Figure 2).

Compaction

Compaction is essentially the conservation of mass of the solid rock material (the mineral component)

Figure 1—Location map of the Piceance basin and the MWX site.
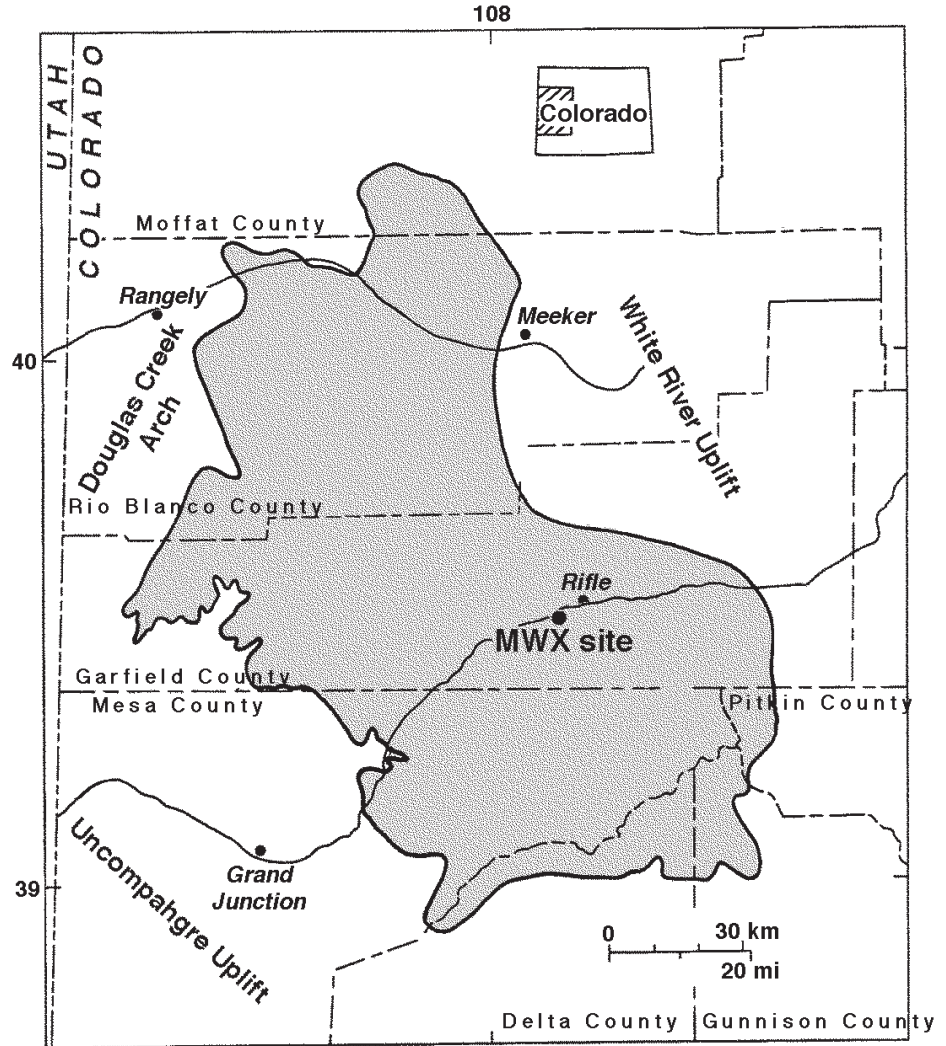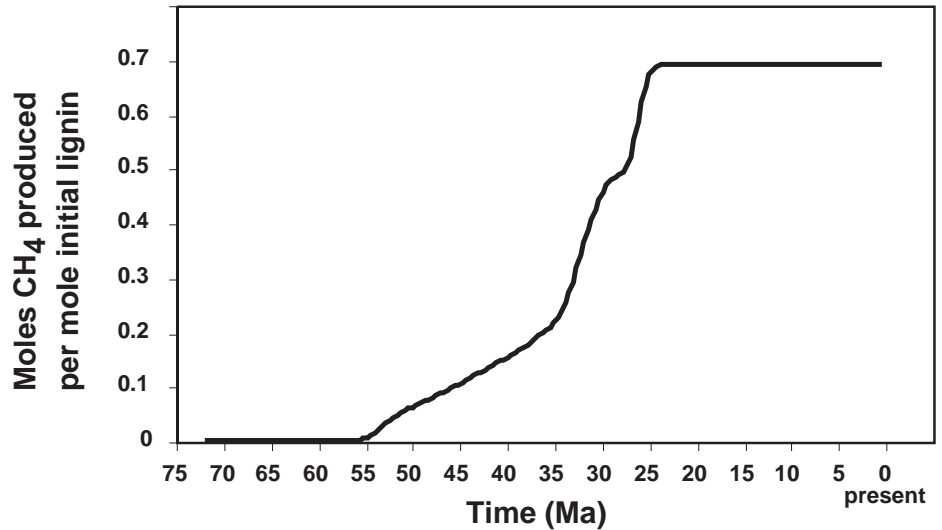

Figure 2—Total methane generation for the paludal interval coal unit, which is the major methane source for this simulation.

as the rock volume is changing due to deformation. In geological terms, it is manifested in the loss of porosity with increasing burial. In the BasinRTM model, it is quantified in terms of the strain rate acting on a given unit mass of rock. The strain rate is calculated as a function of the reversible elastic deformation and the irreversible mechanical deformation. The reversible component can be thought of as a bulk material elastic response to stresses, which are negated when the stresses are removed. The irreversible component, which can be thought of as a viscous response, includes grain sliding (the rearrangement of mineral grains to closer packing) as stresses are applied, pressure-mediated dissolution of mineral grains and associated grain overgrowth (not simulated in this study), and volumetric changes caused by fracture formation and healing. All of the strain rate components are calculated as functions of sedimentary texture, fluid properties, temperature, and stress, which also change over the imposed geologic history of the simulation domain. In this approach, the deformation parameters are functions of texture, stress, and porosity evolution, and hence are strongly coupled and computed self-consistently.

Fracturing

The tensile strength of rock is generally low; therefore, small amounts of tensile stress will result in fracturing (Atkinson, 1987; Atkinson and Meredith, 1987; Pollard and Aydin, 1988). Thus, the formation of fractures is a function of the state of stress (and fluid pressure) and of the rock properties. In the case of isotropic viscoelastic porous media, the ratio of lateral to vertical stress (or more generally, the ratio of least to greatest compressive stress) is strongly dependent on the ratio of shear to bulk viscosity. As the viscosity ratio decreases, for example in fine-grained or poorly lithified sediments, the stress ratio increases. Conversely, as the viscosity ratio increases, for example in coarser grained, more well-lithified sediments, the stress ratio decreases. Hence, coarser grained, more well-lithified strata will fracture more readily. Indeed, this is observed in the Cretaceous Mesaverde strata of the Piceance basin, in which sandstones tend to be fractured, whereas the interbedded and surrounding mudstones are not (Verbeek and Grout, 1984; Pitman and Sprunt, 1986; Lorenz and Finley, 1991).

The stress ratio is also a function of vertical loading, tectonically imposed lateral stresses, and fluid pressure. The vertical stress is a function of the mass of the sedimentary column, gravitational acceleration, and fluid pressure. In the absence of tectonically imposed lateral stresses, as in the case of this one-dimensional simulation study, the lateral stresses are uniform in all directions; therefore, the lateral stress is a function of the vertical stress and the fluid pressure, as well as the rheology. The fluid pressure is a function of compaction rate, fluid composition (aqueous and gas phases), permeability, and temperature, as well as their spatial distributions. It counters the vertical and lateral stresses in equal amounts in all directions. If fluid pressure exceeds least compressive stress, fracturing would likely occur. Hypothetically, because gas generation can contribute to overpressure, it can also contribute to the creation of fractures.

In the BasinRTM simulator, the generation of fractures is the result of a complex nonlinear relationship among stresses, fluid pressure, and rheology. The criterion for fracturing is that the sum of total stress and fluid pressure (effective stress) is negative in the direction of least compressive stress. In other words, the rock is under tensile stress. Fracture characteristics, including length, aperture, and number density, are calculated simultaneously as unique functions of rock texture, the stress tensor, and fluid pressure, as well as the rate of change of stress and pressure.

Fluid Dynamics

In the BasinRTM simulator, the fluid flow rate is described by Darcy flow through porous media, which is a function of permeability, fluid pressure, and fluid density, and satisfies mass balance requirements for the fluid media. Flow rate calculations account for both advective and diffusive components of transport. To account for flow through fractures, permeability and porosity have both matrix and fracture components. The fracture components of porosity and permeability are functions of fracture aperture, length, and number density. Darcy flow is then computed as a function of the total porosity and permeability. In addition, compaction of sediments is accounted for by satisfying mass balance for the changing volume. This affects the fluid pressure and permeability, as well as the cross sectional area through which the fluid volume must be transported.

Two-phase flow is also accounted for in this simulator and thus gas and aqueous phase flow are considered in the Darcy flow equations. CO_2 and CH_4 are generated by the organic diagenesis module, and their solubilities in the aqueous phase are functions of pressure and temperature, according to Henry's Law. As the density of the exsolved gas phase is much smaller than that of the aqueous phase, this will impart a significant effect on the fluid pressure. Transport of the gas phase is described by Darcy flow, but differs from aqueous

phase flow because of differences in relative permeability, viscosity, and density, which are functions of gas saturation and temperature.

BOUNDARY CONDITIONS AND INITIAL DATA

Basin Setting

The geology and the geologic history of the Piceance basin are used to establish appropriate boundary conditions and initial input parameters for the MWX site simulation. The principal gas reservoirs are sandstones in the Upper Cretaceous Mesaverde Group (Iles Formation and Williams Fork Formation) that were deposited between approximately 78 and 66 m.y. ago (Figure 3). The older Iles Formation is marine in origin and consists of several laterally continuous, progradational shallow-marine and shoreface sandstones separated by transgressional tongues of the marine Mancos Shale. The overlying Williams Fork Formation consists of coal-bearing sequences and primarily nonmarine, lenticular sandstones and shales that are interpreted as fluvial deltaic (Collins, 1976). Extensive coal deposits are found in the marine and nearshore units of the Mesaverde Group. These coals are believed to be sources for much of the basin's natural gas reserves (Tyler and McMurry, 1995). These coals tend to overlie marine sandstones in the progradational sequence and are interpreted as swamp deposits directly behind the shoreline. The thickest coal units are in the paludal interval of the lower part of the Williams Fork Formation, overlying the Rollins Sandstone Member of the Iles Formation.

During the Late Cretaceous, as the Mesaverde Group strata were being deposited, rapid subsidence accompanied the deposition of as much as 2000 m of marine and nonmarine sediments. The Piceance basin experienced a period of uplift and erosion at the end of the Cretaceous, forming the present-day boundaries of the basin. Thereafter, the Piceance basin became the site of continued rapid subsidence and deposition of nonmarine sediments of the Tertiary Wasatch and the Green River formations. During this period, compressional forces of the Laramide orogeny created some of the uplifts that define and surround the basin, and deformed the basin to its present asymmetry. The basin reached maximum burial at about 30 Ma, which is probably around the time that significant gas generation commenced. About 20–25 Ma, the basin began to experience uplift, with rapid uplift and erosion dominating the last 10 m.y. of the basin history. Within the last 30 m.y. of the basin history, extensional stresses caused igneous activity in the southern part of the basin, which resulted in an
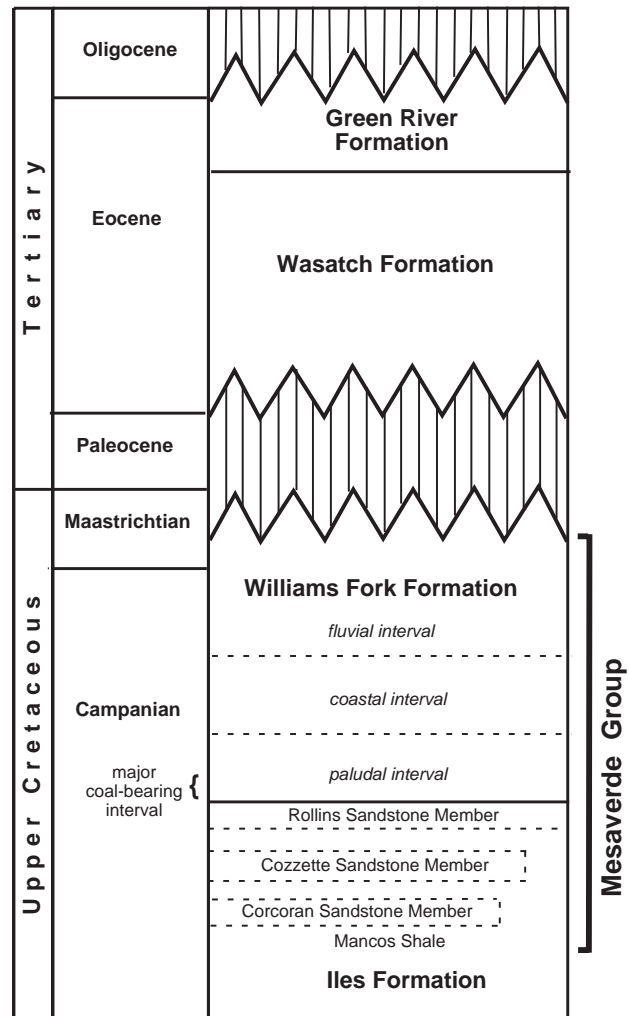

Figure 3—Generalized stratigraphic column of the MWX site representing the stratigraphy used in this study as input for the BasinRTM simulator.

increase in the thermal gradient there. The present-day geothermal gradient at the MWX site may be as high as 45.6°C based on corrected bottom-hole temperatures (Johnson and Nuccio, 1986).

Simulation Input

The Piceance basin history and local MWX site data were distilled into specific input files for the boundary conditions and initial data as follows. The depositional history input (thicknesses of units and ages of contacts) was constructed from well logs such that the sandstone/mudstone ratio, as well as the total coal thickness in the Paludal Interval, is preserved. The sandstones in the Mesaverde Group

were combined such that no single unit is less than 30 m thick to satisfy the minimum thickness for the chosen resolution of the simulation grid. For simplicity, the overlying Wasatch Formation and younger units are left undifferentiated. Table 1 show the input controls on thicknesses of each unit and amounts eroded during periods of uplift, and the ages of the tops of each unit or event.

Lithologic input (grain size distribution) for the Mesaverde Group was modified from petrographic data primarily for coarser grained units in the Mesaverde Group at the MWX site (Multiwell Experiment Project Groups at Sandia National Laboratories and CER Corporation, 1987, 1988, 1989, 1990). These data were compiled and averaged for sandstones in each interval in the Williams Fork Formation, and for each of the three major sandstone units in the Iles Formation. For the lithologic input of sandstone units, the sum of the observed average contents of quartz and feldspar minerals were assigned to the framework grains, and the observed total clay content was assigned to the clay matrix fraction. This composition is then normalized by the program to an assumed depositional porosity of 30%, based on average porosities for poorly to moderately sorted, very fine to medium-grained, wet-packed sands (Beard and Weyl, 1973). Because of the paucity of available data for the composition of these mudstones and shales, the input compositions for this study are loosely based on general mudstone compositional data (Shaw and Weaver, 1965) and on compositional data of the Wasatch Formation mudstones (Hosterman and Dyni, 1972). These compositional fractions are then normalized in the program to account for an assumed depositional porosity of 25%.

Table 1. Input Well File

Unit or Event	Lithology	Age at Top (Ma)	Depth at Top Relative to Present-Day Land Surface (m)	Volume Fraction Kerogen
Erosion		0	0.0	
Hiatus		1.5		
Erosion		8.0	–152	
Hiatus		10.0		
Erosion		20.0	–1464	
Hiatus		22.5		
Wasatch	Silty mudstone	36.0	–1769	0
Wasatch	Silty mudstone	38.0	–1678	0
Wasatch	Silty mudstone	53.0	–762	0
Hiatus		60.0		
Fluvial interval	Mudstone	66.50	1177	0
Fluvial interval	Sandstone	66.95	1359	0
Fluvial interval	Mudstone	67.20	1405	0
Fluvial interval	Sandstone	67.73	1462	0
Fluvial interval	Mudstone	68.11	1505	0
Fluvial interval	Sandstone	68.52	1567	0
Fluvial interval	Mudstone	68.71	1617	0
Fluvial interval	Sandstone	69.59	1801	0
Coastal interval	Shale	69.62	1829	0
Coastal interval	Sandstone	70.20	2060	0
Paludal interval	Shale	70.60	2098	0
Paludal interval	Coal	71.63	2192	1.0
Paludal interval	Sandstone	72.19	2230	0
Paludal interval	Shale	72.34	2252	0
Rollins	Sandstone	72.64	2282	0
Mancos	Shale	72.74	2324	0.1
Hiatus		73.67		
Cozzette	Sandstone	73.98	2387	0
Mancos	Shale	74.05	2438	0.1
Hiatus		74.6		
Corocoran	Sandstone	74.85	2472	0
Mancos	Shale	74.92	2509	0.1

Table 2. Input Lithologic Characteristics

Lithology	Average Observed Porosity (%)*	Assumed Input Porosity (%)**	Sand Fraction Input†	Sand Grain Size Input (radius in mm)	Clay Fraction Input†	Clay Grain Size Input (radius in mm)
Wasatch Formation	NA	25	0.4	0.01–0.05	0.6	0.001
Mesaverde Mudstone & Shale	NA	25	0.3	0.01	0.7	0.001
Fluvial Sandstone	4.8	30	0.57	0.085	0.09	0.001
Coastal Sandstone	8.4	30	0.51	0.06	0.08	0.001
Paludal Sandstone	5.6	30	0.48	0.055	0.09	0.001
Rollins Marine Sandstone	5.1	30	0.53	0.065	0.06	0.001
Cozzette Marine Sandstone	10.7	30	0.68	0.04	0.03	0.001
Corcoran Marine Sandstone	14.5	30	0.52	0.055	0.08	0.001

*Present-day.
**At deposition.
†These values are then normalized against the input porosity to give input mineral volume fractions.

Table 2 shows the present-day and input depositional lithologic characteristics for the Mesaverde sandstones and the generalized characteristics assumed for shales and mudstones. It is probable that a significant fraction of the clay minerals in these sandstones formed during diagenesis (Pitman et al., 1989), and thus it is likely that the depositional clay mineral fraction was smaller than assumed for this model. We suggest that the overestimation of input depositional clays will impede early compaction processes and result in predicted porosities, permeabilities, and overpressures that are too high, but the magnitude of this effect is uncertain without accounting for diagenetic processes in the simulation. Although the BasinRTM simulator does have a module that accounts for inorganic diagenetic reactions, including clay mineral precipitation, it was not within the scope of this study to include this in the modeling. Hence, the clay and framework mineral fractions remain constant over the simulation.

Source rocks are assumed to be coals and coaly mudstones localized in the paludal interval of the Williams Fork Formation and in the upper part of the Iles Formation. Because the depositional environment is generally terrigenous and lignin is likely to be a major terrigenous sedimentary organic component that survives early microbial degradation, the sedimentary organic matter is assumed to be 100% lignin (Table 3). The paludal interval contains approximately 38 m of coal beds. These were unified as a single coal unit in the stratigraphic input (Table 1). The coaly material in the upper part of the Iles Formation is less concentrated, occurring in very thin layers. It is included within the interbedded shales as comprising 10% of the volume fraction (Table 1).

The simulation starts at 75 Ma, during incipient deposition of the Iles Formation. The burial and

Table 3. Other Input Data and Boundary Conditions

Thermal gradient	75–30 Ma	25°C/km
	30 Ma–present	45°C/km
Coal composition	100% lignin	
Bottom boundary	No flux	
Top boundary	Hydrostatic	
Lateral boundary	No flux	

thermal histories for the MWX site from 75 Ma to the present were constructed using published reports, geophysical logs, and vitrinite reflectance modeling (Lorenz, 1985; Johnson and Nuccio, 1986, 1993). The burial history was incorporated with the input stratigraphy in the BasinRTM input well file to account for deposition and burial, hiatus, and uplift and erosion of the simulation domain. The thermal history was incorporated into the model as a changing geothermal gradient: 25°C/km for 75–30 Ma, and 45°C/km for 30 Ma to the present reflecting the changing thermal regime of the region over the last 30 m.y. (Table 3). Figure 4 shows the depth and temperature over time of a point at the bottom of the simulation grid, in the lowermost Mesaverde Group (base of the Iles Formation).

Note that because this study is a one-dimensional simulation, it precludes accounting for differences in lateral stresses due to tectonic activity. Certainly, the compressional and extensional events of the Piceance basin's tectonic history will affect the predicted timing, geometry, and extent of fracturing and fluid flow. Ongoing work will address this by incorporating a lateral deformation history into a three-dimensional simulation at field and basin scales. But for this simulation, stresses from tectonic activity are ignored.
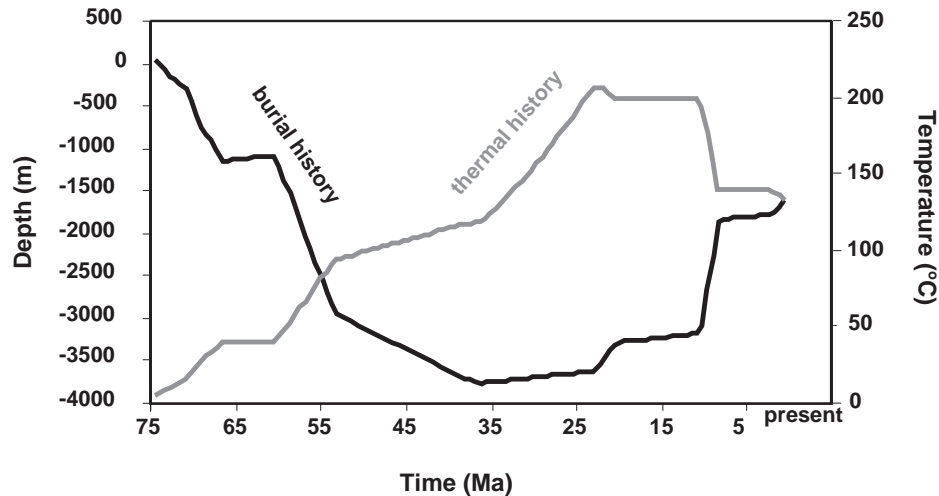
Figure 4—Burial and thermal histories of the MWX site following a point at the bottom of the simulation domain (located at the base of the Iles Formation).

SIMULATION RESULTS

Calibration

This kind of forward model is calibrated by trying to match predicted present-day with observed properties by adjusting input parameters. Very few unequivocal data exist for the history of a basin (examples would include paragenetic sequences of minerals or fracture cross-cutting relationships), so matching is better done with the present-day observations. In this model there are many input parameters and different degrees of confidence in each parameter. In fact, there are probably numerous combinations of input parameters that will predict appropriate present-day properties, each of which would result in a unique predicted basin history. The parameters with the highest degree of uncertainty are those that are modified to make the predicted results fit with the observations. Specifically for this study, the calibration was made by adjusting the equations for irreversible compaction (rock viscosity dependencies) and the permeability law (an exponential function of porosity).

Because this is a one-dimensional simulation, there are some limitations that affect the calibration of the model. As is illustrated in the following section, the match of predicted with observed fluid pressures was not exact and, because of the coupling of processes incorporated in the model, this, in turn, influences the calculations of other predicted present-day properties. Because it is a one-dimensional simulation, only vertical flow is allowed, and not lateral flow. This inhibits fluid pressure reequilibration, so that predicted fluid pressures will likely be higher than true fluid pressures and will take longer to reequilibrate. This model is intended for future use in a three-dimensional simulation, in which case lateral

flux calculations would likely reduce the predicted fluid pressures. Taking this into account, a perfect match of predicted present-day with observed fluid pressures was not sought. We are most interested in using this simulation to examine the interactions of gas generation, compaction, fracturing, and fluid flow during the development of naturally fractured natural gas reservoirs instead of using this simulation to predict the exact locations of producing zones; however, we believe the results are nonetheless relevant.

Predicted Present-Day Characteristics

The depth dependence of key present-day characteristics was predicted and compared with MWX site observations. Figure 5 shows predicted and observed overpressure vs. depth [data from Barrett Resources International (1996, personal communication) and from Spencer (1987)] (Table 4). Overpressure in this study is defined as the aqueous phase pressure minus hydrostatic pressure for that phase (assuming a freshwater composition). Predicted overpressure values diverge from observed values by more than 100 bars in some cases. Excessive predicted overpressure is likely due to a lack of lateral flow in one-dimensional simulations as discussed previously. The top of the predicted overpressure zone is at the top of the Mesaverde Group. Because this interval is the focus of this study, the overlying Wasatch Formation was modeled as a uniform mudstone and is predicted to be uniformly normally pressured at the present time. In fact, the Wasatch Formation is probably hydrodynamically heterogeneous, but the data trend suggests there is likely to be a hydraulic barrier near the top of the Williams Fork fluvial interval and the bottom of the Wasatch Formation.

Figure 5—Predicted present-day and observed overpressure/depth curve for the MWX site [data from Spencer (1987) and from Barrett Resources International].
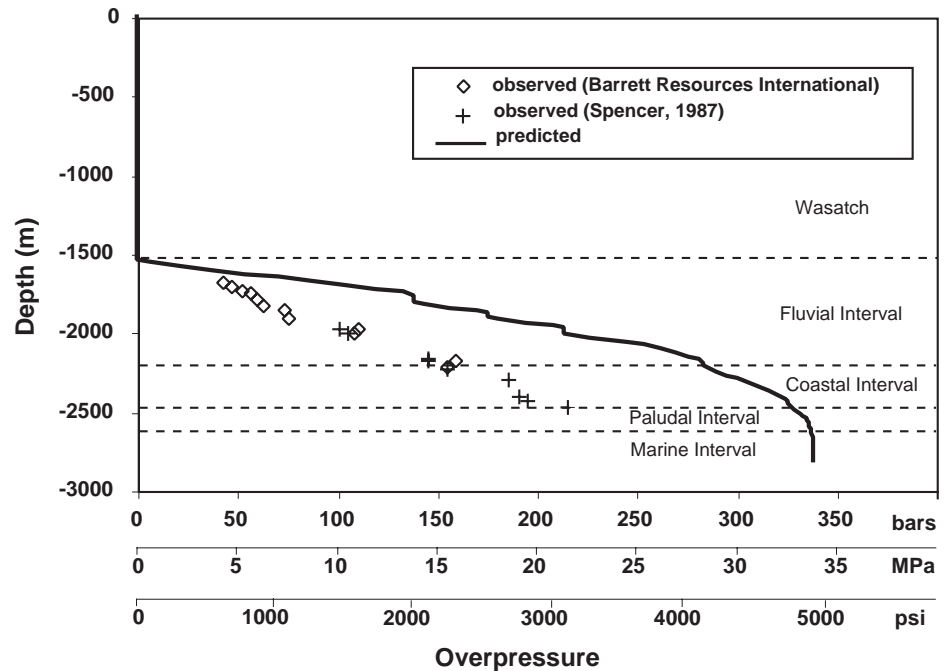
Predicted matrix porosities of sandstone units are also consistently higher than observed (Figure 6). Predicted porosities of shales and mudstones in some cases are higher than those observed in inter-layered sandstones due to undercompaction, for example, in the Rollins and Paludal sandstones. Model-predicted undercompaction may result from two factors. Primarily, the development of excessive overpressure due to the lack of lateral flow in a one-dimensional simulation inhibits mechanical compaction and results in porosities that are too high. In fact, this illustrates the model's ability to capture the coupled compaction/fluid flow processes that result in undercompaction. Secondarily, the effects of chemical compaction are not accounted for in the model. These siliciclastic sediments contain minerals that are sensitive to chemical interaction with water, for example, feldspars, reacting readily to form clay minerals. Indeed, the abundant clay minerals in the sandstones are suggested to be largely diagenetic (Pitman et al., 1989). These minerals are also susceptible to pressure dissolution (Heald, 1955). It is possible, then, that simulating chemical and mechanical compaction would account for additional loss of porosity over the burial history, yielding a closer match with observed porosities.

Predicted matrix permeability, which is an exponential function of porosity, is higher for sandstones than for mudstones, as expected (Figure 7). Observed matrix permeabilities of the sandstone units generally range from 10^{-6} to 10^{-5} d (darcy) for dry

Table 4. Observed Overpressure

Elevation Relative to Sea Level (m)	Overpressure (bars)	
	Barrett Resources	Spencer (1987)
−518	42	
−543	47	
−567	52	
−588	56	
−627	59	
−664	62	
−684	73	
−740	75	
−813	110	100
−834	108	105
−995		145
−1015	159	145
−1049	155	
−1068		155
−1137		185
−1237		190
−1259		195
−1311		215

permeabilities, but for water-saturated conditions the permeabilities may be an order of magnitude lower (data from Multiwell Project Experiment Groups at Sandia National Laboratories and CER Corp., 1987, 1988, 1989, 1990). Thus the predicted present-day matrix permeabilities for the coarser
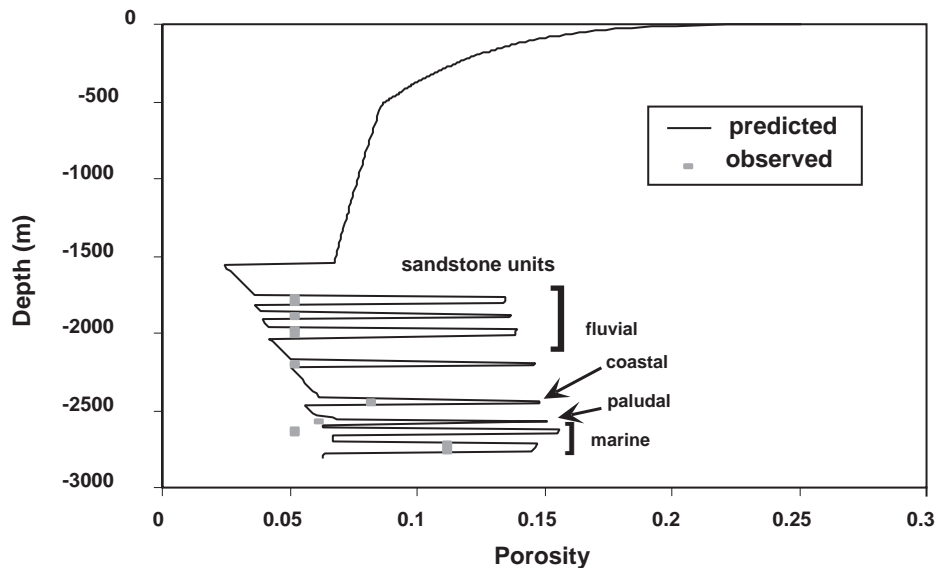
Figure 6—Predicted present-day and observed porosity/depth relationships; observed data indicate averaged data for the coarser grained units. There are no porosity data for the mudstones.
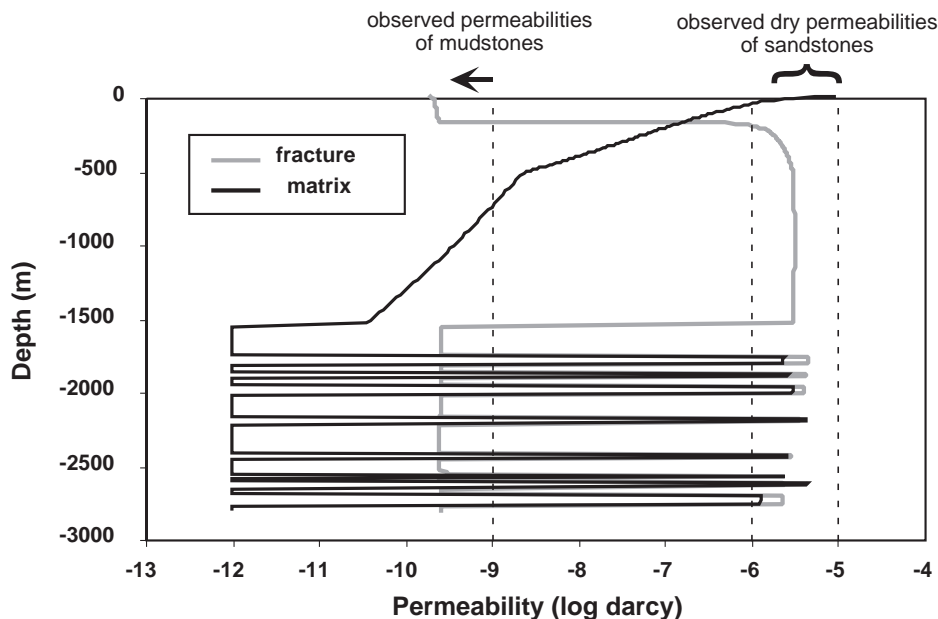

Figure 7—Predicted present-day matrix and fracture permeability vs. depth. Below about 1500 m, maximum permeabilities are associated with sandstone units; the mudstones are predicted to be efficient seals.

grained lithologies may be too high by an order of magnitude (this is a result of overestimated porosity). Observed mudstone permeabilities are estimated to be in the subnanodarcy range (less than 10^{-9}), although such low permeabilities are difficult to measure accurately. Insofar as predicted permeabilities are also in the subnanodarcy range for these lithologies (about 10^{-12} d), they agree with observations.

Figure 7 also shows that predicted fracture permeabilities are higher for sandstones than for mudstones. This illustrates the rheological differences incorporated into the model, which result in greater susceptibility of coarser grained rocks to fracturing. There are no data specifically for fracture permeability at the MWX site, but fractures have been extensively characterized, including frequency, fracture type, and mineralization (Finley and Lorenz, 1988). Assuming that greater fracture frequency or density results in higher fracture permeability, they may be indirectly correlated. Vertical extension fractures are the most numerous type in reservoirs at the MWX site, and

thus they are the dominant control on reservoir permeability (Lorenz and Finley, 1991). These types of fractures are found in sandstones and siltstones but terminate at the mudstone contacts. Hence, the predicted fracture pattern resembles the observed permeability pattern in this aspect.

Predicted fracture permeability generally dominates overall permeability, except near the top of the simulation domain where fractures have not yet formed. Predicted fracture permeability is slightly greater than matrix permeability for most of the sandstones, although it is slightly lower for a few. Finley and Lorenz (1988) noted that the laboratory permeability of rock matrix is one to three orders of magnitude lower than overall permeability indicated by well tests, suggesting that fracture permeability dominates total permeability, although by a larger margin than in these simulation results.

In the model, lateral stresses depend on vertical stress, fluid pressure, and rheology. Figure 8A shows

Figure 8—(A) Predicted present-day lateral stress shown with observed in situ stresses for sandstones and mudstones. The higher correlated stress for mudstones than for sandstones is consistent with observations. (B) Predicted present-day lateral stress shown with predicted vertical stress and overpressure; fracturing is more likely to occur where fluid pressure exceeds lateral stress, as in the sandstones.
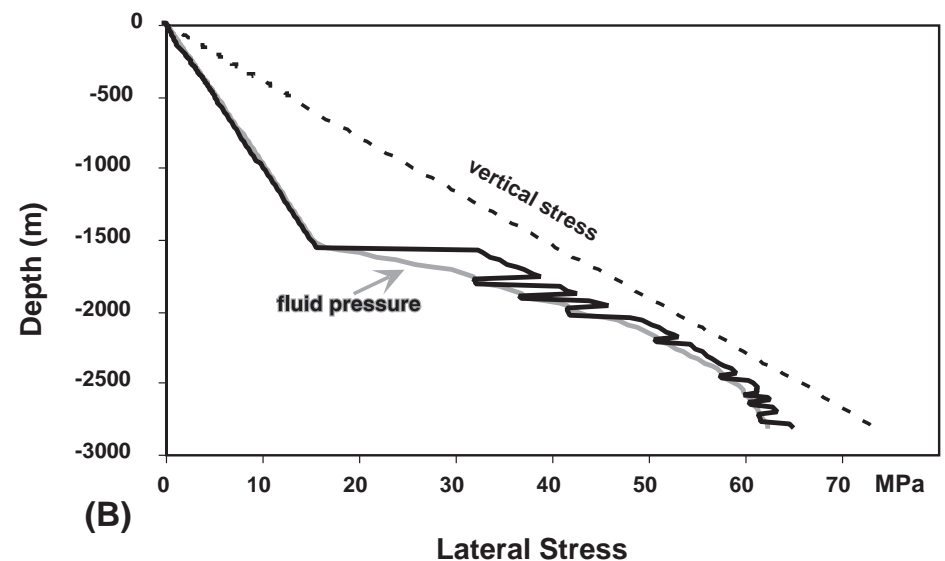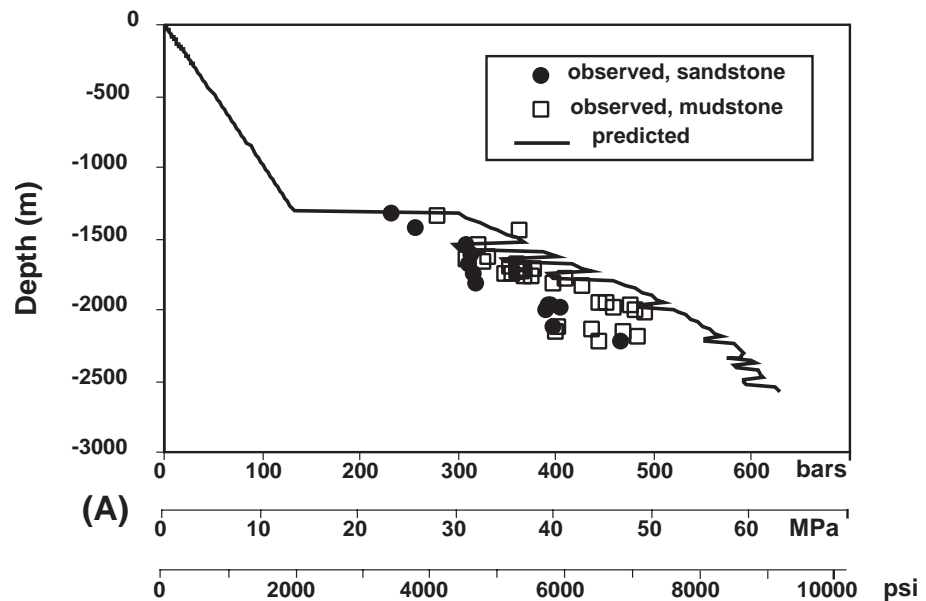
Table 5. In Situ Sandstone Stress*

Depth from Land Surface (m)	In Situ Stress (MPa)
–1321	23.1
–1431	25.7
–1539	30.8
–1615	31.2
–1672	31.2
–1745	31.6
–1819	31.7
–1965	39.4
–1971	39.1
–1986	40.3
–1997	38.9
–2124	39.6
–2216	46.6

*Data from Multiwell Experiment Reports (1987; 1988a, b; 1989).

Table 6. In Situ Mudstone Stress*

Depth from Land Surface (m)	In Situ Stress (MPa)
–1335	27.9
–1438	36.2
–1548	32.1
–1623	33.1
–1652	30.7
–1663	32.5
–1680	36.1
–1701	35.3
–1708	37.8
–1714	36.7
–1723	35.9
–1733	36.4
–1739	35.5
–1752	34.8
–1756	37.5
–1763	36.7
–1785	40.9
–1812	39.7
–1832	42.8
–1944	45.1
–1952	44.4
–1958	47.6
–1991	46.0
–2003	48.1
–2015	49.2
–2113	40.2
–2138	43.6
–2145	46.9
–2156	39.9
–2187	48.3
–2228	44.3

*Data from Multiwell Experiment Reports (1987; 1988a, b; 1989).

that predicted lateral stress generally increases with depth because the vertical stress increases due to greater overburden (Figure 8B). The oscillations in the lower one-half of the predicted lateral stress profile follow stratigraphy; the lateral stresses in sandstones are lower than in adjacent mudstones. This illustrates that in the rheology model, finer grained mudstones behave plastically, and the vertical stress is more easily transferred into lateral stress than in the coarser grained, more brittle sandstones. Observed in situ stresses in sandstones are also lower than in mudstones (Tables 5, 6), although they are generally lower than predicted values by about 10 MPa. The differences between observed and predicted values are similar to the differences in predicted and observed overpressure, suggesting that excess predicted overpressure is causing excessive predicted lateral stresses. This again is a limitation of one-dimensional modeling.

Fracturing in this model occurs when specific stress conditions are met. Because fluid pressure exceeds lateral stress (Figure 8B), fracturing is initiated. Because lateral stress in sandstones is lower and closer to fluid pressure, sandstones are more likely to fracture than the mudstones. In Figure 8B, predicted present-day fluid pressure exceeds lateral stress for the Mesaverde sandstones, indicating that they are fractured as in Figure 7. The dynamics of these stress/fluid pressure relationships, however, are more complex. For example, when the sandstones fracture, the volume increase due to fracturing tends to increase lateral stress in the layer, shifting the lateral stress curve to the right, and the fractures will tend to close. If fluids escape through the fractures and pore fluid pressure decreases, then the lateral stresses will tend to decrease, moving the curve to the left. In this case, the fluid pressure

curve will also tend to move to the left unless there is a means for maintaining the fluid pressure. Potentially, gas generation may help to maintain the relative pore fluid pressure and thus hold fractures open. Once fracturing is initiated, whether the fractures remain open or start to close will depend on the relative decreases in lateral stress and fluid pressure, and whether the fluid pressure continues to exceed lateral stress.

The model predicts that present-day gas saturation exists from the lower part of the Mesaverde fluvial interval (incorporating the deepest sandstone unit in this interval) to the bottom of the simulation domain (Figure 9). Gas saturation is defined as the volume of pore space occupied by gas phases as opposed to the aqueous phase. Figure 9 shows that Mesaverde mudstone lithologies are predicted to have higher gas saturations than the interbedded sandstone lithologies. Because the mudstones have lower permeabilities,

Figure 9—Predicted present-day gas saturation vs. depth; average predicted gas saturation of 20% in sandstones is lower than indicated by the predominant range of observed water saturation values (30–60%).
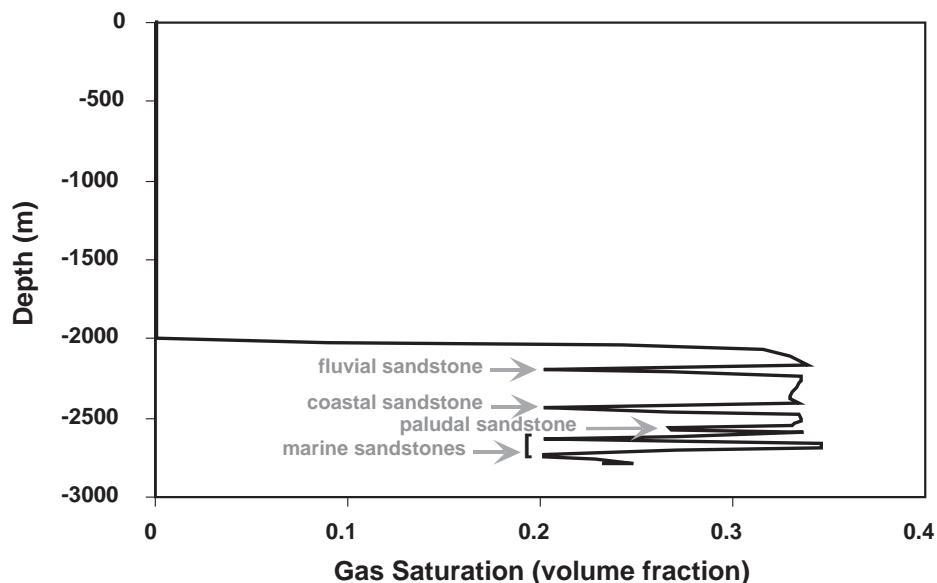
they have lower relative permeabilities to gas, and thus higher residual gas saturation, although total gas content in the sandstones is greater. Laboratory data on core water saturations show a wide range of values: 20–75% for the fluvial interval, 22–95% for the coastal interval, and 36–55% for the paludal interval. The majority of measurements are in the 30–60% range. If gas saturations can be estimated from the water saturations, then the bulk of gas saturations would range from 40 to 70%, which is higher than predicted for either sandstones or mudstones.

The differences between predicted and observed characteristics can be largely attributed to insufficient predicted compaction, which is a result of the inadequacy of one-dimensional simulations to describe fluid flow during sedimentary basin development, and is possibly the result of neglecting the compaction effects of pressure solution processes. With respect to these limitations, predicted values are within an acceptable range for the purpose of this study, and the simulations generally capture observed patterns of the reservoir characteristics, illustrating the model's utility for examining the interactions of RTM processes during basin development.

Dynamics of Reservoir Development

To show how basin processes interact through time, and more specifically the effects of gas generation on reservoir development dynamics, the overpressure history of the simulated MWX site is examined with respect to various processes. The patterns of simulated overpressure histories of the

Mesaverde stratigraphic units are similar, and differ primarily in magnitude of overpressure as a function of depth. Figure 10 shows that the timing of overpressuring and reequilibration events are essentially the same for the marine Cozzette sandstone, the coastal interval sandstone, and the uppermost sandstone in the fluvial interval, except that the onset of overpressuring is delayed for shallower units. The magnitude of overpressure is greatest for the deepest unit, the marine Cozzette sandstone, and least for the shallowest unit, a fluvial interval sandstone, largely because of differences in vertical stress. The most distinct difference between overpressure histories occurs toward the end of the simulation, in which the deeper two units experience a rapid decline in overpressure, followed by a slower decline; the shallowest of these sandstones experiences a rapid decline in overpressure, then an increase followed by a plateau, which starts to decline at the very end of the simulation. This difference can be explained by the lack of gas saturation in all but the deepest of the fluvial interval sandstone units (Figure 9), which allows a more rapid deflation of overpressure, and a subsequent period of compaction accompanied by overpressure there. This figure shows negligible overpressure in the overlying Wasatch Formation, indicating that a good permeability seal has formed below it, separating it from the overpressured, uppermost fluvial interval mudstones. For the remainder of this analysis the coastal interval sandstone unit will be used to illustrate reservoir development dynamics because it overlies the coal-bearing paludal interval (the dominant gas source in this simulation), and is thus
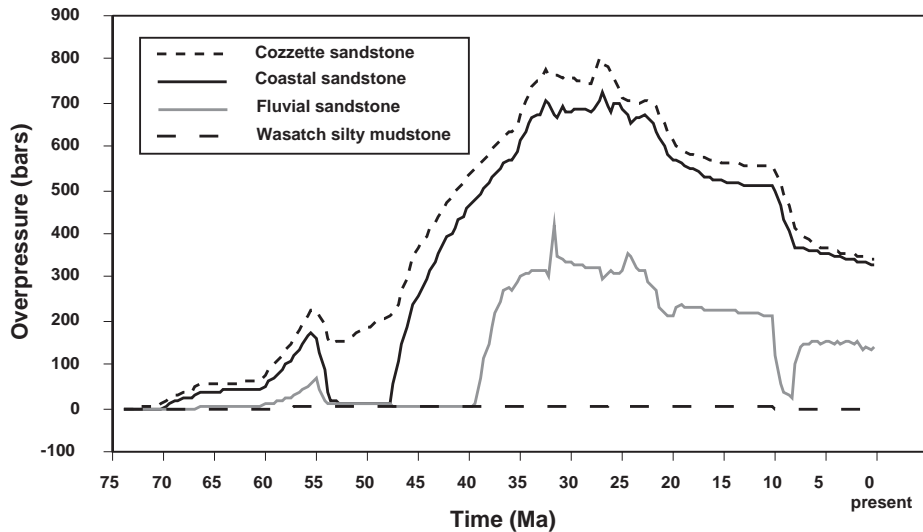
Figure 10—Simulated overpressure histories of the marine Cozzette sandstone, the coastal interval sandstone, a fluvial interval sandstone, and the silty mudstone of the Wasatch Formation. For the Mesaverde Group sandstones, the patterns are similar and the magnitude of overpressure increases with depth of strata.

expected to be strongly influenced by gas generation and migration.

Early in the simulation history, overpressure in the coastal interval sandstone correlates with and can be attributed to mechanical compaction. The onset of overpressuring mirrors the burial curve from the beginning of the simulation to about 57 Ma (Figure 11). During this period, burial causes compaction, which results in loss of permeability. In this case, overpressure results from compaction operating more rapidly than fluids can be transported out of the pore spaces. Similarly, from about 20 Ma to the end of the simulation, the pattern of declining overpressure mirrors the pattern of uplift. In this case, uplift is accompanied by erosion and loss of overburden, as well as cooling and contraction of pore fluids, which reduce the stresses on the pores, allowing pressure to decline.

Between 55 and 53 Ma the fluid pressure drops and distinctly does not correlate with the burial history. This period of fluid pressure reequilibration occurs during continued rapid burial; hence, a process other than compaction must be strongly controlling fluid pressures at this point. In addition, from about 35 to 25 Ma, during the maximum burial, overpressure fluctuations do not correlate with and are likely not directly related to the burial history. These periods will be examined with respect to fracturing, gas generation and saturation, and the behavior of the interlayered mudstones.

Figure 12 compares matrix and fracture permeability histories with the overpressure history of the coastal interval sandstone. Early in the simulation, matrix permeability dominates. At about 57 Ma, fracturing of the sandstone commences and fracture permeability increases rapidly until about 40 Ma, where it essentially plateaus, with a minimal

increase through time. In this simulation, final fracture and matrix permeability values are similar and thus control total permeability equally. The fracture permeability of the mudstone directly overlying the coastal interval sandstone is shown in this figure, as well. Early enhanced fracture permeability from about 55 to 47 Ma represents a period of fracturing and is followed by fracture closing. Fracture permeability fluctuations occur between about 32 and 24 Ma and represent shorter repetitive cycles of fracture opening and closing. Periods of lowest fracture permeability represent periods when this mudstone forms an efficient seal above the coastal interval sandstone.

The drop in overpressure in the coastal interval sandstone at about 56 Ma appears to correlate temporally with the onset of fracturing within this unit and with fracturing of the overlying coastal interval mudstone. The fracture closing in the overlying mudstone at about 47 Ma also correlates well with the onset of significant overpressuring in the coastal interval sandstone. From about 53 to 48 Ma, fracturing in the sandstone and the overlying mudstone allow fluids to escape from the sandstone, causing rapid fluid pressure reequilibration. During this period, the fractures remain open allowing normal fluid pressures to prevail despite the increasing overburden. After 48 Ma, a critical stress state is reached and fractures in the mudstones close, creating an effective seal above the sandstone; subsequently, overpressure in the sandstone starts to increase.

The fracture permeability of the coastal interval sandstone remains high for the remainder of the simulated history, indicating that once fractured, the fractures do not close. In this case, the rheological model is maintaining very low lateral stress in

Figure 11—Comparison of simulated overpressure history and burial history of the coastal interval sandstone showing that compaction correlates with overpressure at the early and late times, whereas other factors (fracturing, methanogenesis) dominate at intermediate times.
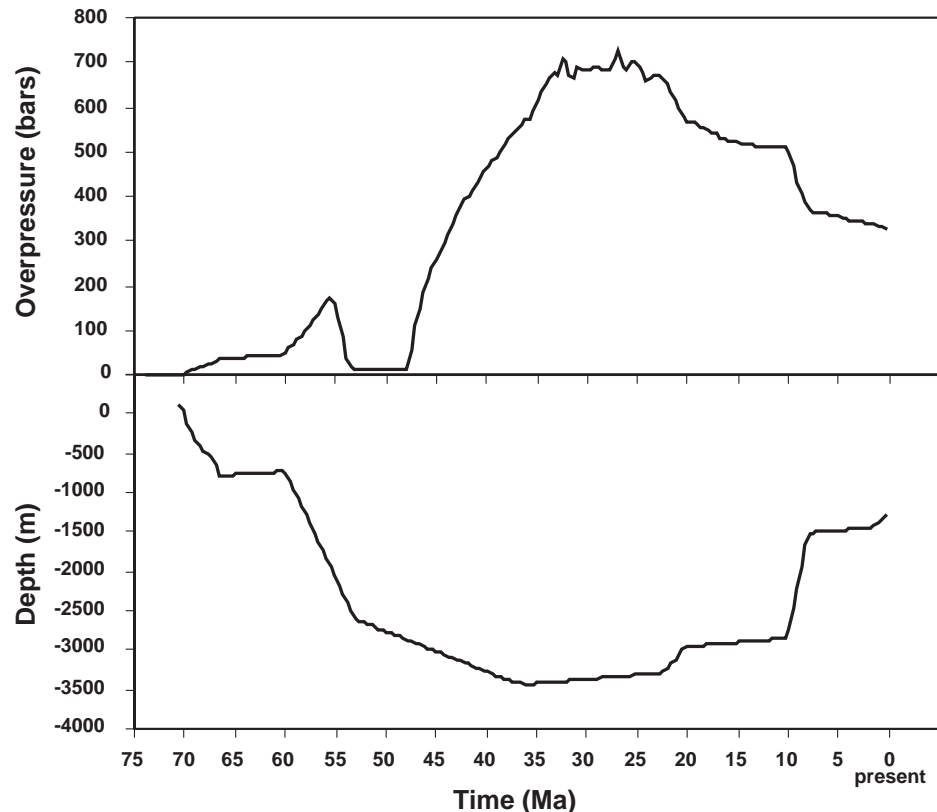
the sandstone. Because the predicted lateral stress remains very close to the predicted fluid pressure even under conditions of minimal overpressure (53–48 Ma), the fracture permeability remains high. This is not necessarily how all sandstones would behave under such conditions. In the Piceance basin, although it is likely that there are well-fractured sandstones under low fluid pressure conditions, there are also sandstones that are relatively unfractured. Here, the rheological model describes conditions under which the sandstones are relatively susceptible to fracturing.

The fluctuations in fracture permeability in the coastal interval mudstone from 32 to 24 Ma appear to correlate with small fluctuations in overpressure when overpressure is at its greatest magnitude. In this case, the overpressure, which is of substantial magnitude, exceeds least compressive stress and initiates fracturing in the coastal interval mudstone. As fluids are released, the overpressure diminishes, allowing the fractures to close. This illustrates that the model captures the close coupling of fracturing and overpressuring processes. The cyclic nature of overpressuring-induced fracturing is schematically shown in Figure 13 and discussed in Dewers and Ortoleva (1994), Maxwell (1997), and Ortoleva (1994).

These results illustrate the dynamic relations between fracturing, compaction, and fluid pressure. Because the generation of gas contributes to the creation and maintenance of overpressure, it may also affect fracturing. Figure 2 shows the total methane generated in the paludal interval coal unit, which is the primary methane source rock, according to the gas generation model. Methanogenesis starts at about 55 Ma and ceases around 25 Ma, when uplift commences and temperatures begin to decrease, and the gas generation potential of the source rock is predicted to be largely exhausted. This figure indicates that the total amount of methane produced over the simulation is almost 0.7 moles per mole of unreacted lignin. Figure 14 compares the fluid pressure history of the coastal interval sandstone with gas saturation (pore volume occupied by gas phase generated from underlying source rocks) there. Starting at about 52 Ma, after incipient maturation of the underlying source rock (the paludal interval coal), gas is initially transported into the sandstone dissolved in pore fluids. Aqueous methane concentration increases as more gas is generated by maturing source rocks, and as pore fluid migrates upward into the sandstone from compacting and overpressuring source rocks below. Aqueous methane concentration continues
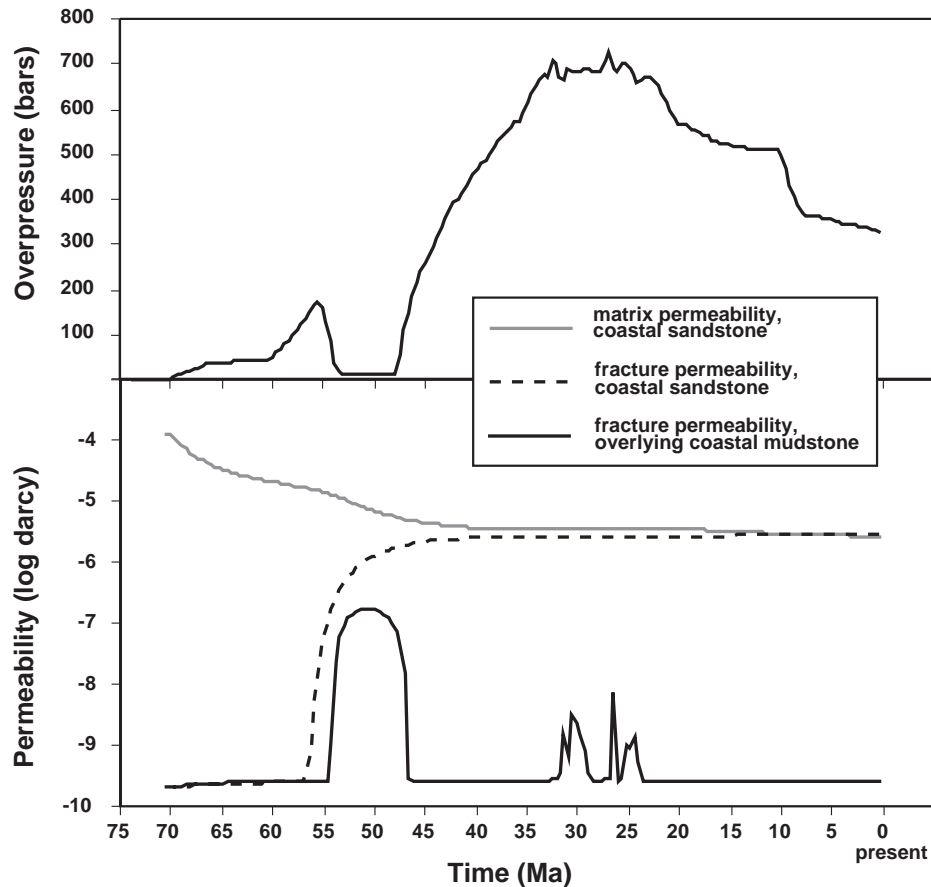
Figure 12—Comparison of simulated overpressure history and matrix and fracture permeabilities of the coastal interval sandstone, and fracture permeability of the overlying coastal interval mudstone. The overpressure history of the sandstone is affected by fracturing within it, but more dominantly by fracturing of the overlying mudstone.

to increase until its peak at about 25 Ma. At this time, aqueous methane concentration begins to decrease and the free gas phase forms. The gas phase is exsolving from the aqueous phase because uplift and erosion are decreasing the confining stresses and decreasing the solubility of the gas in the aqueous phase. Aqueous methane continues to decline for the remainder of the simulation, and gas saturation is maintained at about 20%.

Because gas saturation in the coastal interval sandstone appears to occur only as the system is in overpressure decline, it does not appear that there is a direct relationship between the generation of the gas phase and the creation of overpressure or fracturing in that unit; however, a comparison of this simulation to one in which there is only an aqueous fluid phase suggests three important, yet subtle, effects of gas generation. First, Figure 15 shows that the magnitude of maximum overpressure is somewhat lower in the simulation without gas generation and saturation. Although the coastal interval sandstone is not gas saturated before 25 Ma, gas generation in the source rocks is significant during maximum burial, and resulting gas saturations in

units underlying the coastal interval sandstone may be contributing to the overall fluid pressures in surrounding units. Second, on the overpressure curve for the single-phase simulation (no gas saturation) (Figure 15), two negative spikes occur at 21 and at 9 Ma, the second reaching underpressure. These drops in overpressure are followed by rapid increases in overpressure. In the absence of gas saturation, uplift and erosion (resulting in cooling and a decrease in confining stresses) cause an accelerated decline in fluid pressures. When fluid pressures drop so significantly, compaction processes operate again, allowing the fluid pressures to rebuild when uplift and erosion slow down (from 9 Ma to the present). Hence, an important role of gas generation is the sustenance of overpressure by gas saturation while the basin is experiencing uplift and erosion. Finally, the fluctuating fluid pressures occurring during maximum overpressure (35–25 Ma) in the two-phase system do not occur in the single-phase system. Although there is no direct correlation of this phenomenon with gas saturation in this same strata, the absence of a gas phase in the single-phase simulation suggests that it is indirectly

**Figure 13—Dynamic and cyclic
nature of overpressuring and
fracturing processes in fractured
compartments. As fluid pressure
exceeds lateral stress, the rock is
more likely to fracture (1 and 2).
As fracturing occurs, permeability
increases, fluids leak out of the
compartment, and fluid pressure
starts decreasing (3). Finally,
as fractures heal, permeability
decreases until fluid pressures
can build up again, completing
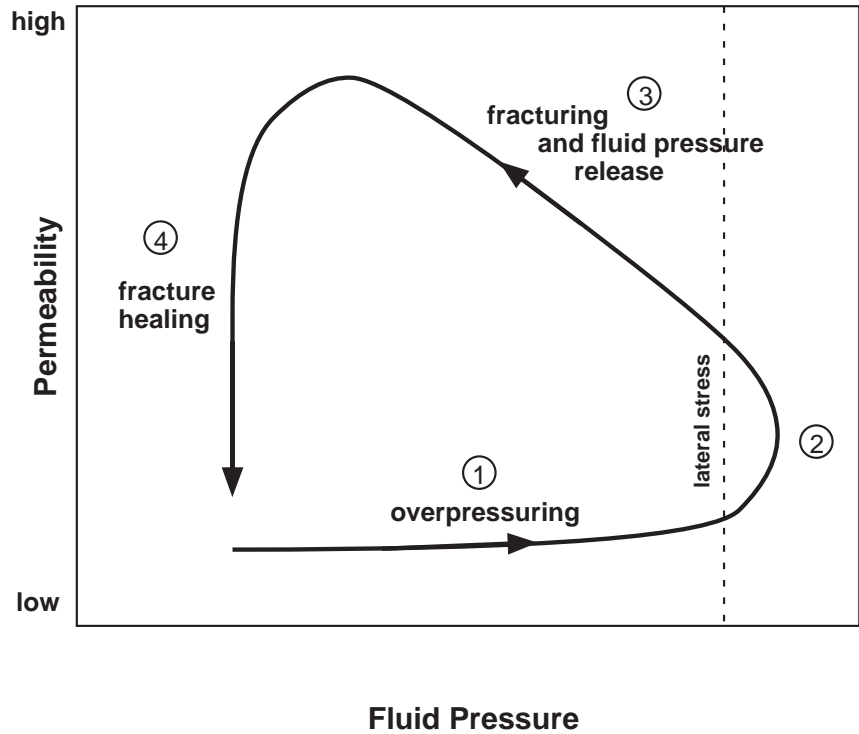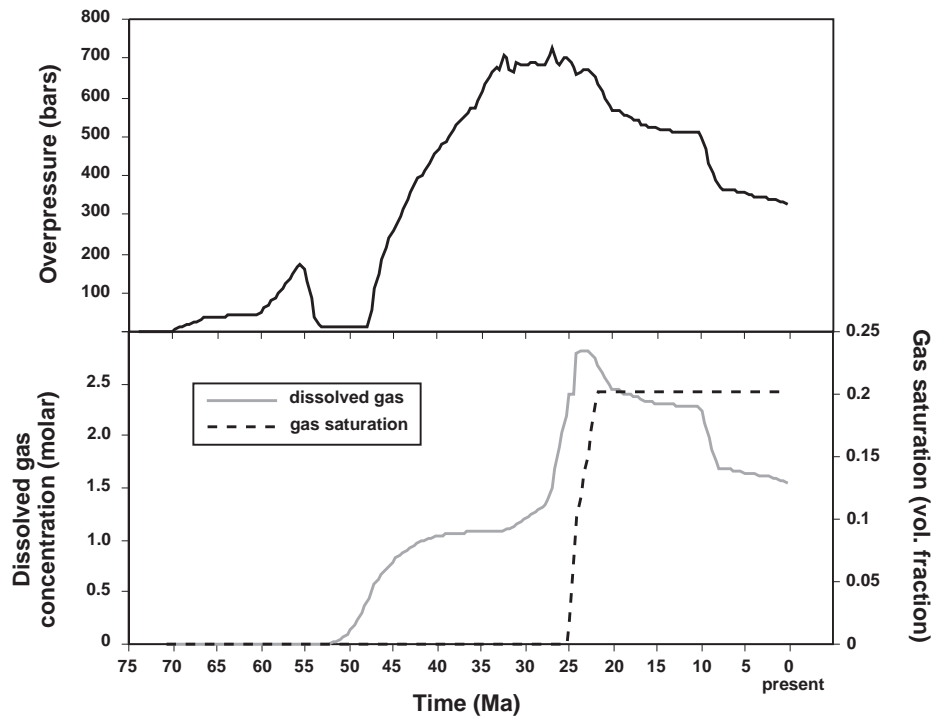the cycle (4).**

**Figure 14—Comparison of
simulated overpressure
history with dissolved
gas concentration and gas
saturation in the coastal
interval sandstone.
Gas saturation in the
coastal interval sandstone
has no simple correlation
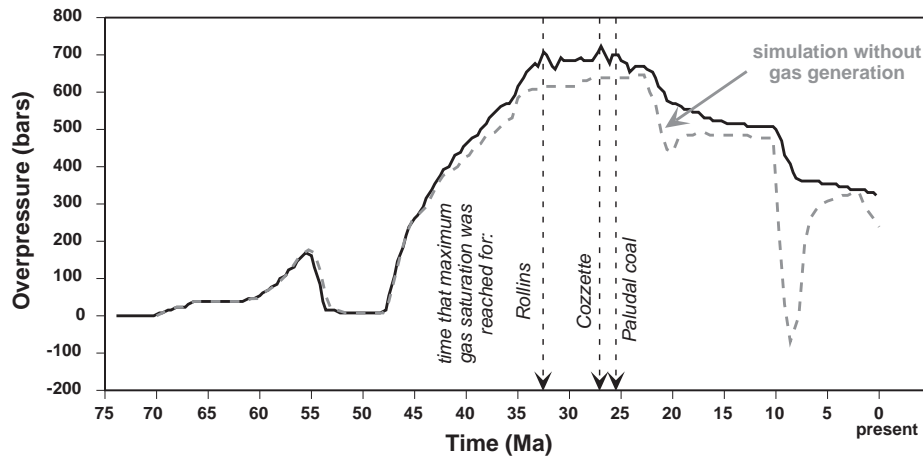with the overpressure
history.**

Figure 15—Comparison of overpressure history in the coastal interval sandstone with and without methanogenesis and multiphase flow.

related to gas saturation. Indeed, a comparison with gas saturations of units underlying the coastal interval sandstone shows that the overpressure spikes in the coastal interval sandstone may be correlated with the timing that underlying Cozzette and Rollins sandstones and the paludal interval coal achieve maximum gas saturation. This suggests that gas saturation in one unit affects the overall stresses acting on other units. In this case, it causes fracturing in the coastal interval mudstone. In these ways, the simulation suggests that gas generation affects fracturing and the timing, geometry, and therefore characteristics of flow conduits and seals. Thus gas generation is integrally involved in the development of reservoirs in which natural gas is contained.

DISCUSSION

This modeling study suggests how RTM processes in sedimentary basins interact and why predicting reservoir characteristics in these settings is so difficult. In these dynamic systems, numerous processes may be acting simultaneously and are affected by imposed conditions to different degrees, resulting in reservoir properties that change temporally and spatially. For example, this model suggests that under relatively shallow (<2 km) burial conditions, compaction processes may contribute significantly to excess fluid pressure, which, in turn, may affect fracturing processes. In addition, the model accounts for the coupling of processes, which illustrates the weakness of simple cause-and-effect relationships. For example, the model suggests that in the case of the coastal interval mudstone, because overpressure contributes to fracturing, the fractures allow the expulsion of the fluids and reequilibration of fluid pressure and the subsequent closing of the fractures. These complexities would

preclude the prediction of reservoir characteristics through simple correlations of present-day properties, and illustrate the utility of forward numerical modeling of RTM processes.

Under the assumptions presented by this model, this study also suggests that gas generation may have two significant consequences for overpressuring and fracturing in systems like the Piceance basin. The first is that the resulting overpressure affects stress conditions to promote fracturing. Gas saturation in one unit, by contributing to the overpressure, may result in fracturing episodes in nearby units, such as predicted for the coastal interval mudstone. This may then result in cyclic fluctuations in fluid pressure of the higher permeability reservoir units, as fluid pressure is released then subsequently builds (Figure 13). This has implications for the transport of gases because the fracturing episodes may open conduits for both the aqueous phase and the gas phase.

The second consequence of gas generation is the maintenance of elevated pore fluid pressure during uplift and erosion of the Piceance basin. These results support Spencer's (1987) assertion that gas generation may be responsible for present-day elevated pore fluid pressures while the basin is otherwise experiencing pressure decline. Our results suggest that without gas generation, significant underpressure is predicted to occur during uplift and erosion. Indeed, locally observed underpressure in the Piceance basin may reflect a lack of gas saturation during uplift in those locations. This is in agreement with the qualitative rule of thumb that natural gas can be correlated with surviving overpressure. By contributing to excess fluid pressure, generated and migrated gases may affect reservoir properties by preventing compaction and fracture closing, and thus helping to maintain permeability in gas saturated units. In these ways gas generation

may play a role in creating the reservoirs in which it is sequestered.

These results also suggest that the overall effect of gas generation on reservoir development is subtle and indirect when considered in the context of all RTM basin processes. Rheologic properties may be more important in terms of fracture development because different rocks may respond quite differently under similar imposed stress conditions. Also, mechanical compaction processes may contribute to the development of significant overpressure in the absence of, or before, significant gas generation, via the expulsion of fluids from more rapidly compacting mudstones into more permeable sandstones, and the formation of low-permeability flow barriers surrounding sandstones. This significant overpressure, in turn, may affect fracturing processes as discussed.

Sedimentary basins are dynamic and complex systems, and in cases such as the Piceance basin, predicting reservoir characteristics is inherently difficult. Although this one-dimensional forward model of the MWX site is not intended to be used to unequivocally predict productive zones in the Piceance basin, it can be used to illustrate the effects of the multiple and coupled processes and the relative effects of individual processes on reservoir development and characteristics. With continued model refinement and testing on three-dimensional simulations, it is possible that this forward modeling technique may become applicable as a tool for predicting reservoir characteristics.

REFERENCES CITED

Atkinson, B. K., 1987, Introduction to fracture mechanics and its geophysical applications, *in* B. K. Atkinson, ed., Fracture mechanics of rock: San Diego, Academic Press, p. 1–26.

Atkinson, B. K., and P. G. Meredith, 1987, Experimental fracture mechanics data for rocks and minerals, *in* B. K. Atkinson, ed., Fracture mechanics of rock: San Diego, Academic Press, p. 477–525.

Beard, D. C., and P. K. Weyl, 1973, Influence of texture on porosity and permeability of unconsolidated sand: AAPG Bulletin, v. 57, p. 349–369.

Cartwright, J. A., 1994, Episodic basin-wide fluid expulsion from geopressured shale sequences in the North Sea basin: Geology, v. 22, p. 447–450.

Collins, B. A., 1976, Coal deposits of the Carbondale, Grand Hogback and Southern Danforth Hills coal fields, eastern Piceance basin, Colorado: Quarterly Report of the Colorado School of Mines, v. 71, no. 1, 138 p.

Dewers, T., and P. J. Ortoleva, 1994, Nonlinear dynamical aspects of deep basin hydrology: fluid compartment formation and episodic fluid release: American Journal of Science, v. 294, p. 713–755.

Finley, S. J., and J. C. Lorenz, 1988, Characterization of natural fractures in Mesaverde core form the Multiwell Experiment: Sandia National Laboratory Report SAND88-1800, 90 p.

Heald, M. T., 1955, Stylolites in sandstones: Journal of Geology, v. 63, p. 101–114.

Hedberg, H. D., 1974, Relation of methane generation to undercompacted shales, shale diapirs, and mud volcanics: AAPG Bulletin, v. 58, p. 661–673.

Hoak, T. E., and A. L. Klawitter, 1997, Prediction of fractured reservoir production trends and compartmentalization using an integrated analysis of basement structures in the Piceance basin, Western Colorado, *in* T. E. Hoak, A. L. Klawitter, and P. K. Blomquist, eds., Fractured reservoirs: characterization and modeling: Rocky Mountain Association of Geologists 1997 Guidebook, p. 67–102.

Hosterman, J. W., and J. R. Dyni, 1972, Clay mineralogy of the Green River Formation, Piceance Creek basin, Colorado—a preliminary study: U.S. Geological Survey Professional Paper 800-D, p. 159–163.

Hunt, J. M., 1990, Generation and migration of petroleum from abnormally pressured fluid compartments: AAPG Bulletin, v. 74, p. 1–12.

Johnson, R. C., and V. F. Nuccio, 1986, Structural and thermal history of the Piceance Creek basin, western Colorado, in relation to hydrocarbon occurrence in the Mesaverde Group, *in* C. W. Spencer and R. F. Mast, eds., Geology of tight gas reservoirs: AAPG Studies in Geology 24, p. 165–205.

Johnson, R. C., and V. F. Nuccio, 1993, Surface vitrinite reflectance study of the Uinta and Piceance basins and adjacent areas, eastern Utah and western Colorado—implications for the development of Laramide basins and uplifts: U.S. Geological Survey Bulletin, 1787-DD, 38 p.

Lorenz, J. C., 1985, Tectonic and stress histories of the Piceance Creek basin and the MWX site, from 75 million years ago to the present: preliminary report: Sandia National Laboratories Report, SAND-84-2603.

Lorenz, J. C., and S. J. Finley, 1991, Regional fracturing II: fracturing of Mesaverde reservoirs in the Piceance basin, Colorado: AAPG Bulletin, v. 75, p. 1738–1757.

Lorenz, J. C., N. R. Warpinski, and L. W. Teufel, 1993, Rationale for finding and exploiting fractured reservoirs, based on the MWX/SHCT-Piceance basin experience: Sandia National Laboratory Report SAND93-1342, 150 p.

Luo, X. R., and G. Vasseur, 1996, Geopressuring mechanism of organic matter cracking: numerical modeling: AAPG Bulletin, v. 80, p. 856–874.

Maubege, F., and I. Lerche, 1994, Geopressure evolution and hydrocarbon generation in a north Indonesian basin: two-dimensional quantitative modeling: Marine and Petroleum Geology, v. 11, p. 104–120.

Maxwell, J. M., 1997, The physical chemistry and nonlinear dynamics of compartment formation in sedimentary basins: Ph.D. dissertation, Indiana University, Bloomington, Indiana, 407 p.

Multiwell Experiment Project Groups at Sandia National laboratories and CER Corporation, 1987, Multiwell Experiment final report: I. The marine interval of the Mesaverde Formation: Sandia National Laboratories Report, SAND87-0327.

Multiwell Experiment Project Groups at Sandia National laboratories and CER Corporation, 1988, Multiwell Experiment final report: II. The paludal interval of the Mesaverde Formation: Sandia National Laboratories Report, SAND88-1008.

Multiwell Experiment Project Groups at Sandia National laboratories and CER Corporation, 1989, Multiwell Experiment final report: III. The coastal interval of the Mesaverde Formation: Sandia National Laboratories Report, SAND88-3284.

Multiwell Experiment Project Groups at Sandia National laboratories and CER Corporation, 1990, Multiwell Experiment final report: IV. The fluvial interval of the Mesaverde Formation: Sandia National Laboratories Report, SAND89-2612.

Ortoleva, P. J., 1994, Geochemical self-organization: New York, Oxford University Press, 411 p.

Payne, D. F., 1998, A new, fully-coupled, reaction-transport-mechanical approach to modeling the evolution of methane reservoirs in the Piceance basin: Ph.D. dissertation, Indiana University, Bloomington, Indiana, 180 p.

Pitman, J. K., and E. S. Sprunt, 1986, Origin and distribution of fractures in lower Tertiary and Upper Cretaceous rocks,

Piceance basin, Colorado, and their relation to the occurrence of hydrocarbons, *in* C. W. Spencer and R. F. Mast, eds., Geology of tight gas reservoirs: AAPG Studies in Geology 24, p. 221–233.

Pitman, J. K., C. W. Spencer, and R. M. Pollastro, 1989, Petrography, mineralogy, and reservoir characteristics of the Upper Cretaceous Mesaverde Group in the east-central Piceance basin, Colorado: U.S. Geological Survey Bulletin, 1787-G, 31 p.

Pollard, D. D., and A. Aydin, 1988, Progress in understanding jointing over the past century: Geological Society of America Bulletin, v. 100, p. 1181–1208.

Roberts, S. J., and J. A. Nunn, 1995, Episodic fluid expulsion from geopressured sediments: Marine and Petroleum Geology, v. 12, p. 195–204.

Shaw, D. B., and C. E. Weaver, 1965, The mineralogical composition of shales: Journal of Sedimentary Petrology, v. 35, p. 213–222.

Spencer, C. W., 1987, Hydrocarbon generation as a mechanism for overpressuring in Rocky Mountain region: AAPG Bulletin, v. 71, p. 368–388.

Tyler, R., and R. G. McMurry, 1995, Genetic stratigraphy, coal occurrence, and regional cross section of the Williams Fork Formation, Mesaverde Group, Piceance basin, northwestern Colorado: Colorado Geological Survey Open File Report 95-2.

Tyler, R., A. R. Scott, W. R. Kaiser, H. S. Nance, and R. G. McMurry, 1996, Geologic and hydrologic controls critical to coalbed methane producibility and resource assessment: Williams Fork Formation, Piceance basin, northwest Colorado: Gas Research Institute Topical Report GRI-95/0532, 398 p.

Verbeek, E. R., and M. A. Grout, 1984, Fracture studies in Cretaceous and Paleocene strata in and around the Piceance basin, Colorado: preliminary results and their bearing on fracture controlled natural-gas reservoir at the MWX site: U.S. Geological Survey Open-File Report 84-156, 30 p.

Wang, C., and X. Xie, 1998, Hydrofracturing and episodic fluid flow in shale-rich basins—a numerical study: AAPG Bulletin, v. 82, p. 1857–1869.

ABOUT THE AUTHORS

Dorothy Payne

Dorothy Payne is a hydrologist with the U.S. Geological Survey (USGS) Water Resources Division. After receiving an undergraduate degree in geology from Bryn Mawr College, she worked for a few years as a hydrologist with the USGS. She received her M.S. degree and Ph.D. (1998) in geochemistry from Indiana University working under Professor Peter Ortoleva. Her research interests include reaction- and solute-transport modeling of petroleum and hydrologic systems.

Kagan Tuncay

Kagan Tuncay is a postdoctoral fellow in the Laboratory for Computational Geodynamics at Indiana University. He received his B.S. and M.S. degrees from Middle East Technical University in Ankara, Turkey, and then his Ph.D. from Texas A&M in 1995. His current research interests include rock rheology, multiphase flow, fracture mechanics, and nonlinear processes in geosciences.

Anthony Park

Anthony Park is a research associate in the Laboratory for Computational Geodynamics at Indiana University. He completed his M.S. degree and Ph.D. in geochemistry at Indiana University working under Professor Peter Ortoleva. He has done internships and contract work for Amoco and Mobil, and was a postdoctoral fellow at the Institut Français du Petrole in 1995 and 1996. His research interests include dynamic nonlinear systems in geology and basin and reservoir modeling.

John Comer

John Comer is geochemistry section head at the Indiana Geological Survey. After receiving his Ph.D. from University of Texas at Austin, he worked as a research geochemist for Amoco Production Company. From 1975 to 1988 he was a professor at the Department of Geosciences at the University of Tulsa. His research interests include deposition and diagenesis of organic-rich rocks and the physical chemistry of low-temperature aqueous systems.

Peter Ortoleva

Peter Ortoleva is a Distinguished Professor of Chemistry and Geological Sciences at Indiana University (IU). He has a Ph.D. in applied physics from Cornell University, did postdoctoral research at Massachusetts Institute of Technology in physical chemistry, and has received Sloan and Guggenheim awards. Since joining the IU faculty in 1975, his work has focused on reaction transport modeling of geological systems with an emphasis on basin modeling, and he is currently working on applications to fractured and salt-tectonic–related reservoirs.